ISSN 0021-3640, JETP Letters, 2013, Vol. 97, No. 6, pp. 367–377. © Pleiades Publishing, Inc., 2013.
Original Russian Text © B.B. Straumal, S.G. Protasova, A.A. Mazilkin, G. Schütz, E. Goering, B. Baretzky, P.B. Straumal, 2013, published in Pis'ma v Zhurnal Eksperimental'noi i Teoreticheskoi Fiziki, 2013, Vol. 97, No. 6, pp. 415–426.

Ferromagnetism of Zinc Oxide Nanograined Films

B. B. Straumal[a–c, *], S. G. Protasova[a, d], A. A. Mazilkin[a, d], G. Schütz[d], E. Goering[d], B. Baretzky[c], and P. B. Straumal[e]

[a] *Institute of Solid State Physics, Russian Academy of Sciences, ul. Akademika Ossipyana, Chernogolovka, Moscow region, 142432 Russia*

** e-mail: straumal@issp.ac.ru*

[b] *National Research Technological University MISiS, Leninskii pr. 4, Moscow, 119049 Russia*

[c] *Karlsruher Institut für Technologie, Institut für Nanotechnologie, Hermann-von-Helmholtz-Platz 1, 76344 Eggenstein-Leopoldshafen, Germany*

[d] *Max-Planck-Institut für Metallforschung, Heisenbergstrasse 3, 70569 Stuttgart, Germany*

[e] *Baikov Institute of Metallurgy and Materials Science, Russian Academy of Sciences, Leninskii pr. 49, Moscow, 119991 Russia*

Received February 11, 2013

The reasons for the appearance of ferromagnetic properties of zinc oxide have been reviewed. It has been shown that ferromagnetism appears only in polycrystals at a quite high density of grain boundaries. The critical size of grains is about 20 nm for pure ZnO and more than 40 μm for iron-doped zinc oxide. The solubility of manganese and cobalt in zinc oxide increases significantly with a decrease in the size of grains. The dependences of the saturation magnetization on the concentrations of cobalt, manganese, and ion are nonmonotonic. Even if the size of grains is below the critical value, the ferromagnetic properties of zinc oxide depend significantly on the texture of films and the structure of amorphous intercrystallite layers.

DOI: 10.1134/S0021364013060143

Dietl et al. [1] theoretically predicted for the first time that oxides (in particular, zinc oxide) doped with "magnetic" atoms (e.g., Co, Mn, or Fe) can have ferromagnetic properties with the Curie temperature above room temperature [1]. That work stimulated numerous experimental investigations whose authors attempted to detect predicted ferromagnetism. Some experimental groups observed well-reproducible ferromagnetism in ZnO, but other teams reliably stated that it was absent. Ferromagnetism in zinc oxide is of such a large interest because, owing to the high-temperature ferromagnetism in zinc oxide, which is a transparent broadband semiconductor, this material is very promising for spintronics, because it opens the possibility of the magnetic-field control of the electric properties of the material and the electric-field control of its magnetic properties. However, as was mentioned in review [2], the presence or absence of high-temperature ferromagnetism in zinc oxide is controlled by defects of the crystal structure and its source remains unclear in many respects. For this reason, investigation of the effect of grain boundaries on ferromagnetism in zinc oxide is one of the most topical subjects of the modern physics of condensed matter and physical materials sciences.

Below, we review our studies [3–13] of thin zinc oxide nanocrystalline films (both pure and doped with cobalt, manganese, or iron) obtained by the so-called liquid ceramics method. A mixture of liquid organic acids and metal ions was deposited on a substrate made of an aluminum foil or a sapphire single crystal with the (102) orientation and was then dried at 150°C. As a precursor for the fabrication of pure zinc oxide films, we used zinc butanoate (II) dissolved in an organic solvent with a zinc concentration of 1 to 4 kg/m^3. To synthesize zinc oxide films doped with cobalt, manganese, or iron, the zinc butanoate solution was mixed with the cobalt, manganese, or iron butanoate solution in the corresponding proportions. Then, deposited layers were subjected to pyrolysis in air or in argon at 500, 550, and 600°C. Oxidation of the layer of organic acids occurred simultaneously with the pyrolysis of this layer. As a result, thin films of pure or doped zinc oxide were obtained. The resulting films were pore-free and contained zinc oxide equiaxial nanograins (Fig. 1). They were slightly green and transparent. The thickness of the films was determined using electron-probe X-ray microanalysis and transmission electron microscopy. This thickness was between 50 and 200 nm. The concentrations of cobalt, manganese, and iron in the films varied from 0 to 52 at %, from 0 to 47 at %, and from 0 to 40 at %, respectively. The concentrations of cobalt, manganese, and iron in the doped oxide films were measured using atomic absorption spectroscopy in a Perkin–Elmer spectrometer and using the electron-probe X-ray microanalysis with a Tescan Vega TS5130 MM scanning electron microscope equipped with an energy dispersion spec-

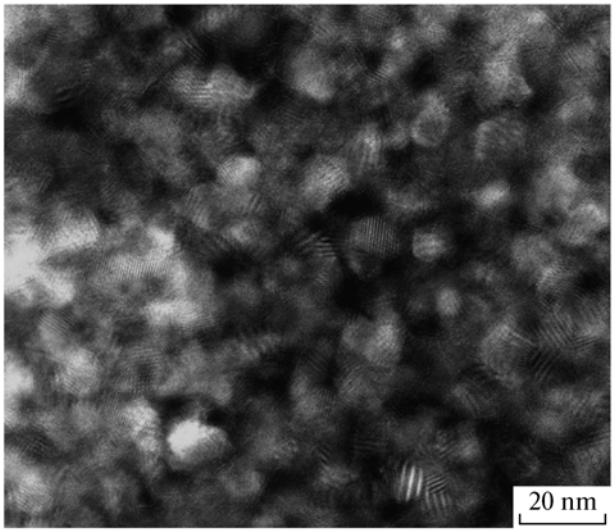

Fig. 1. Dark field electron microscope image of a thin zinc oxide nanocrystalline film obtained using the liquid ceramics method [3].

trometer (Oxford Instruments). Transmission electron microscopy studies were performed using a JEM-4000FX microscope at an accelerating voltage of 400 kV. Transmission electron microscopy was used to study the crystal structure of the film, particularly at the inner interfaces, and to seek possible particles of pure cobalt or manganese oxide. In addition, it was used to measure the grain size in pure and doped zinc oxide films. The X-ray diffraction was studied using a Siemens diffractometer with a graphite monochromator and a gas flow detector at Fe $K\alpha$ radiation. The size of grains in the samples under study was calculated from the angular dependence of the line broadening [5] and appeared to be (10 ± 2) nm. The magnetic properties were measured using a SQUID interferometer (Quantum Design MPMS-7 and MPMS-XL). The magnetic field was applied parallel to the plane of the sample. The diamagnetic signal generated by a sample holder and a substrate was accurately subtracted from the magnetization curves.

INCREASE IN THE TOTAL SOLUBILITY OF THE SECOND COMPONENT IN A POLYCRYSTAL WITH DECREASING GRAIN SIZE

When the concentration of the dopant c in two- and multicomponent alloys increases, the solubility limit is reached at a certain concentration c_s. The second phase in the bulk of the grain appears above c_s. With a further increase in c, only the amount of the second phase increases, whereas the concentration in the first phase remains equal to c_s. The bulk solubility limit increases with the temperature. The simplest method of the measurement of c_s is the observation of the variation of the lattice parameter of the solid solution using, e.g., X-ray diffractometry. The lattice parameter varies continuously (it can both increase and decrease) with an increase in c up to c_s. At $c > c_s$, the lattice period remains unchanged and intensity maxima corresponding to the second phase appear on the diffraction pattern.

When the alloy contains surfaces of interfaces enriched in the second component, the total concentration of this second component c_t is higher than its concentration in the solid solution in the bulk of the grain c_v. The difference between c_t and c_v increases with the specific area of outer surfaces and interfaces (e.g., with a decrease in the grain size). If the grains are sufficiently small, the difference between c_t and c_v can become measurable. This phenomenon is due to the fact that X-ray diffractometry detects only diffraction from bulk phases. The component located in thin surface layers or layers at the interfaces remains undetected by this diffractometry. Intensity peaks on the X-ray diffraction pattern appear only when the coherently scattering region is quite large (the grain size is approximately 5 nm or larger). X-ray diffractometry makes it possible to simultaneously measure the grain size from the angular dependence of the width of the peak.

McLean [14] assumed that the total solubility c_{sa} in fine-grained materials is higher than the bulk solubility limit c_s [14] and calculated this difference for the Fe–C system with the grain size from 1 to 10 μm for the case of the simple grain-boundary segregation of the Langmuir type [14]. According to many works [15–20], $c_{sa} > c_s$ in micro- and nanograined materials. However, X-ray diffractometry studies of the shift of solubility $c_{sa} - c_s$ as a function of the grain size d are very difficult. To the best of our knowledge, such studies were not performed. Zinc oxide provides a good opportunity for such studies.

The solubility limits of cobalt and manganese in zinc oxide nanocrystalline films with a grain size of 20 nm were determined from variation of the zinc oxide lattice spacing with an increase in the concentration of these elements. The period of the zinc oxide lattice increases linearly when the cobalt concentration increases to 33 at % (Fig. 2a) [4]. Above 33 at % Co, the second phase Co_2O_3 with the cubic structure appears and the period of the wurtzite lattice of zinc oxide ceases to increase with the cobalt concentration. This means that the solubility limit c_{sa} of cobalt in the zinc oxide thin films is 33 at % at 550°C (film synthesis temperature). The solubility limit of manganese is approximately 30 at % (Fig. 2b) [13]. Comparison with the previous data (Fig. 2b) shows that, the smaller the grains, the slower the increase in the lattice period with the manganese concentration and the higher the concentration at which the solubility limit is reached;

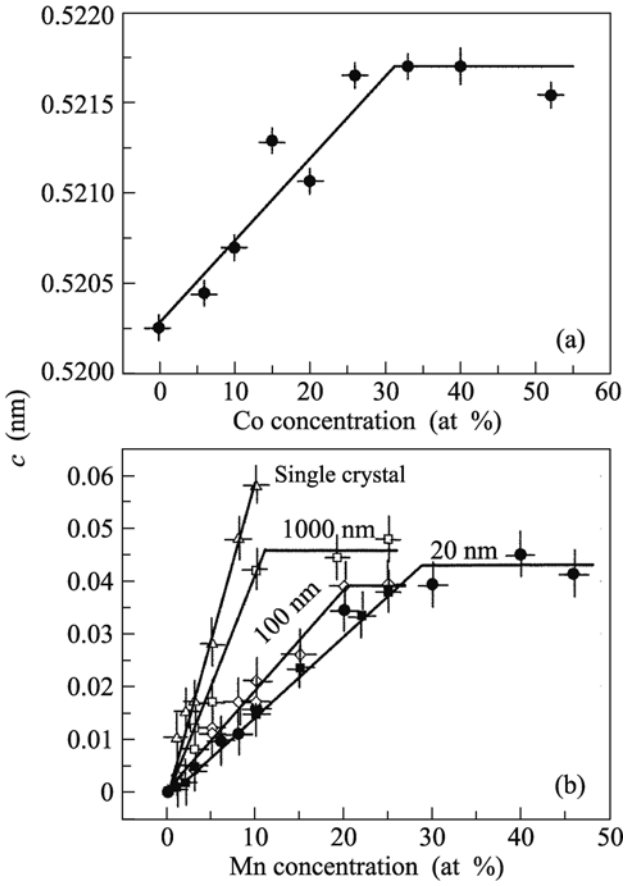

Fig. 2. (a) Lattice parameter c in cobalt-doped zinc oxide films versus the cobalt concentration [4]. (b) Period of a zinc oxide lattice versus the manganese concentration for various sizes of grains [5].

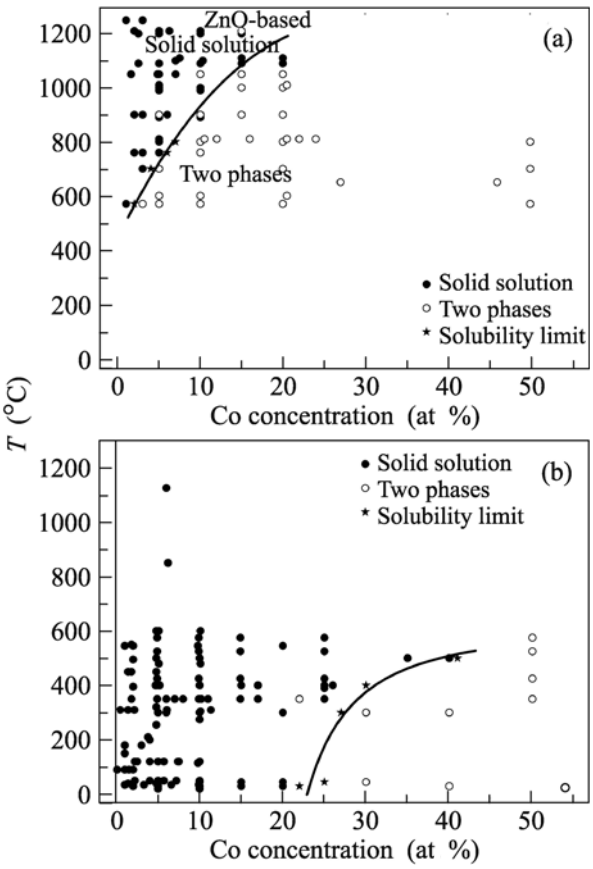

Fig. 3. Solubility limit of cobalt in zinc oxide polycrystals with the grain size (a) larger than 1000 and (b) smaller than 20 nm [4]. The closed and open symbols correspond to single- and two-phase samples, respectively. Stars mark the solubility limit.

i.e., the second phase Mn_3O_4 appears. We attribute this phenomenon to the adsorption of the second component at grain boundaries.

About 2000 experimental works concerning low-doped semiconductors were reported after theoretical predictions made in [1]. To identify ferromagnetism in doped zinc oxide, it is important to test the absence of any particles of the second phase that can affect the magnetic properties of the sample. Thus, each published work studying ferromagnetism in zinc oxide presents the data on the concentration of a dopant and reports the presence or absence of the second phase. Using these data, we plotted the lines of the solubility limit of cobalt and manganese in zinc oxide for various grain sizes (Figs. 3 and 4) [4, 5]. Figure 3 shows the solubility limit lines of cobalt for grain sizes larger than 1000 nm and smaller than 20 nm with experimental points. Figure 4 shows the solubility limit lines of cobalt and manganese for various grain sizes without experimental points. It can be clearly seen that the complete solubility of both cobalt and manganese increases strongly with a decrease in the grain size.

If grain boundaries are absent in the samples and only the developed outer surface is present (nanopowders, nanowires, tetrapods), the complete solubility also increases with a decrease in the particle size, but this increase is much slower than that in the case of polycrystals (with grain boundaries) [4, 5]. Estimates of the adsorption capacity of grain boundaries and outer surface show that an absorption layer with a capacity of 2–4 ML appears on outer surfaces and more than 10 ML of cobalt or manganese appear at grain boundaries [4, 5].

Thus, the accumulation of cobalt and manganese at grain boundaries and free surfaces drastically shifts the solubility limit of these elements in zinc oxide toward higher concentrations. In particular, the complete solubility of cobalt in the bulk of zinc oxide at 550°C does not exceed 2 at %, whereas the complete solubility of cobalt in a nanocrystalline sample with a grain size of less than 20 nm is 33 at %. The solubility of manganese at 550°C increases from 12 to 40 at %. At the same grain size, the displacement of the solubility boundary in a polycrystal with grain boundaries is

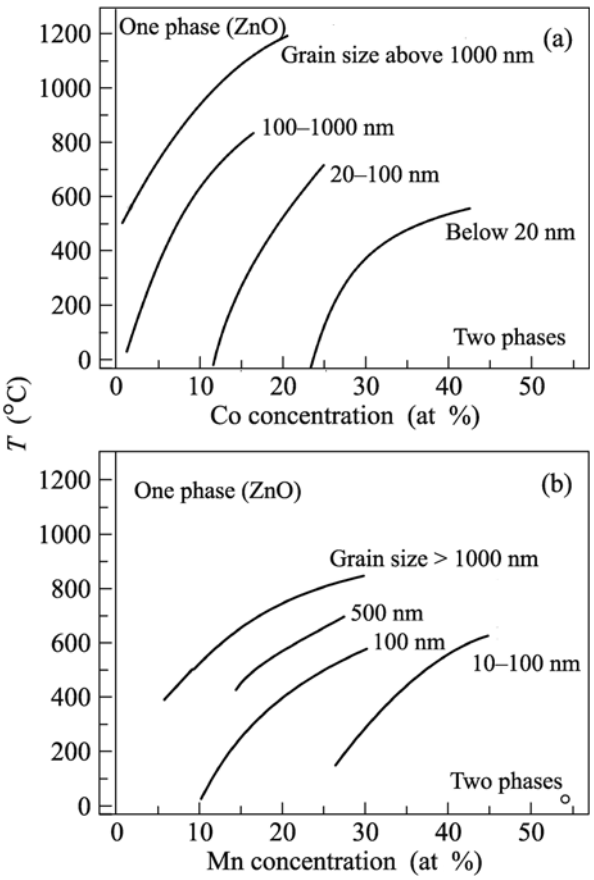

Fig. 4. Solubility limit of (a) cobalt [4] and (b) manganese [5] in zinc oxide polycrystals with various grain sizes.

larger than that in an unsintered powder without grain boundaries. This means that the amount of cobalt or manganese that can be accumulated at grain boundaries is larger by a factor of 2–4 than that in free surfaces. Consequently, the phase diagrams of materials with the grain size smaller than 1000 nm should be reconsidered. Particularly drastic changes in phase diagrams can be expected for the grain size smaller than 100 nm.

CRITICAL GRAIN SIZE FOR THE APPEARANCE OF FERROMAGNETIC PROPERTIES IN ZINC OXIDE

The results of about 2000 published experimental works devoted to search for ferromagnetism in pure and doped zinc oxide are contradictory. The analysis of the reported data shows that pure and doped zinc oxide single crystals, as well as the samples obtained by sintering of usual coarse-grained powders (with the particle size larger than 10 μm), always remain diamagnetic or paramagnetic. The samples obtained using pulsed laser ablation almost always exhibit ferromagnetism at room temperature. The zinc oxide samples synthesized by the methods of "wet chemistry" or chemical vapor deposition (CVD) have intermediate properties. They can be both paramagnetic and ferromagnetic.

We assumed that the existence of ferromagnetic properties in zinc oxide correlates with the specific area s_{GB} of grain boundaries in unit volume. We determine this quantity using the data of published works on ferromagnetism in zinc oxide both pure [6] and doped with manganese [6], cobalt [12], and iron [13]. The results of these calculations for pure and manganese-doped zinc oxide are shown in Fig. 5 in (temperature–specific area s_{GB}) coordinates, where the temperature is the annealing or sample synthesis temperature.

The results certainly indicate that the ferromagnetic properties of pure and doped zinc oxide samples depend on the specific area of grain boundaries. The samples have the ferromagnetic properties only when the specific area of grain boundaries exceeds a certain threshold value s_{th}. Free surfaces, even if their specific area is large and zinc oxide particles are very small, but grain boundaries in a sample are absent, do not lead to ferromagnetism. If zinc oxide nanoparticles or nanowires are not sintered altogether and do not contain grain boundaries, they also have no ferromagnetic properties. Similar results were also obtained for zinc oxide samples doped with cobalt, manganese, and iron. Thus, the presence of manganese, cobalt, or iron is not a necessary condition for the appearance of ferromagnetic properties in zinc oxide. Even pure zinc oxide can be ferromagnetic. In this case, the small grain size (or high specific area s_{GB}), rather than doping with magnetic atoms as was thought initially [1], is of critical importance. Nevertheless, the presence of manganese, cobalt, or iron in the zinc oxide lattice promotes the transition to the ferromagnetic state and increases the critical grain size (Fig. 5). In particular, the authors of a number of works where the specific area of grains fell between the critical sizes for pure and manganese-doped zinc oxide observed paramagnetic properties in pure zinc oxide and ferromagnetic properties in manganese-doped samples [21, 22]. The effects of the additions of manganese, cobalt, and iron on the critical value s_{th} are different. In particular, for pure zinc oxide, $s_{th} = 5.3 \times 10^7$ m^2/m^3 [6], whereas for cobalt-doped ZnO, $s_{th} = 1.5 \times 10^6$ m^2/m^3 [12]. In the case of doping with manganese, the ferromagnetic properties appear beginning already with $s_{th} = 2.4 \times 10^5$ m^2/m^3 [6]. Iron promotes to the greatest extent the appearance of ferromagnetic properties in zinc oxide. They appear already at $s_{th} = 5 \times 10^4$ m^2/m^3, which corresponds to the effective grain size of about 40 μm (in pore-free polycrystals with equiaxial crystallites) [13].

Figure 6 shows the magnetization curves at room temperature (in units of 10^{-3} μ_B/f.u.) for pure zinc

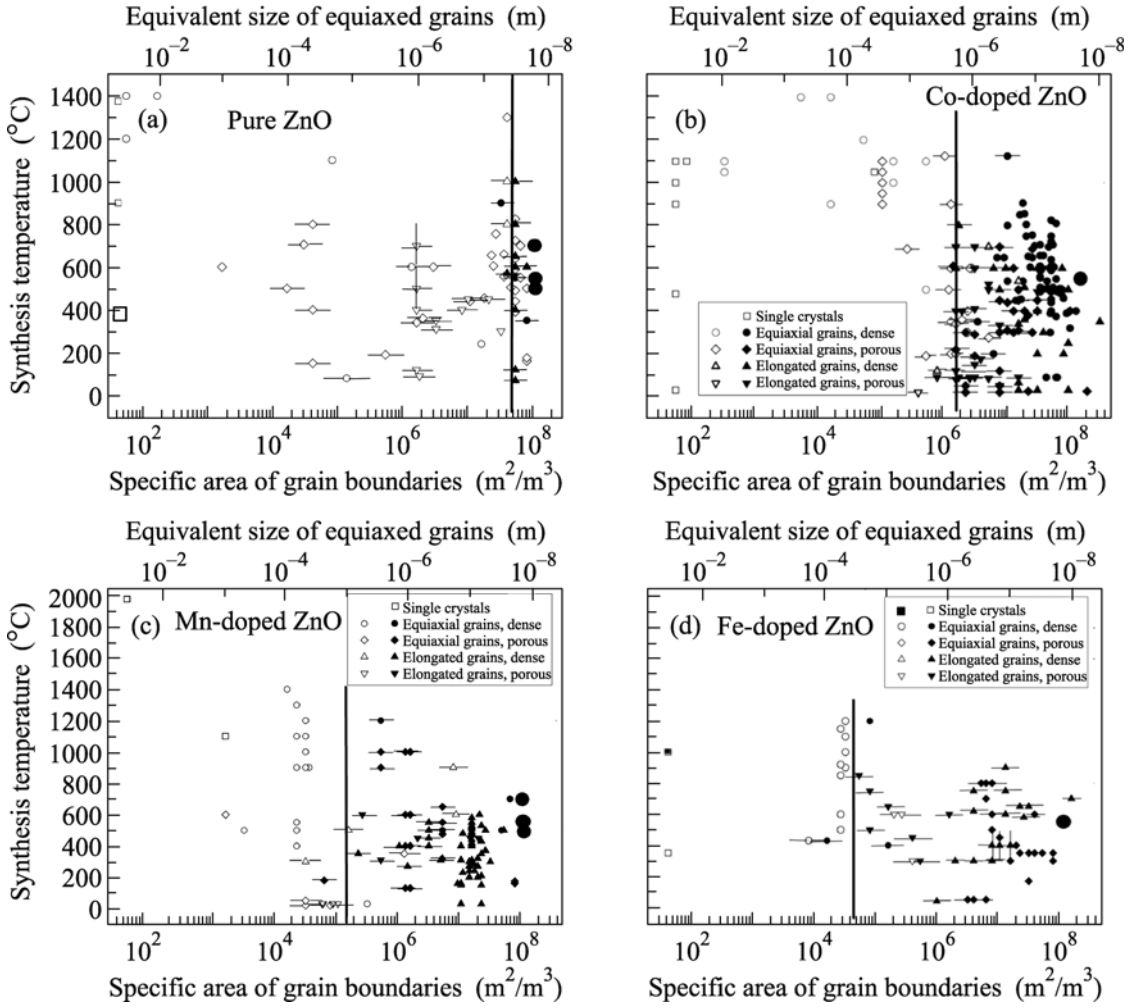

Fig. 5. (Full symbols) Ferromagnetic and (open symbols) paramagnetic or diamagnetic behaviors of (a) pure zinc oxide [6] as well as zinc oxide doped with (b) cobalt [12], (c) manganese [6], and (d) iron [13] versus the specific area of grain boundaries s_{GB} (ratio of the area of the boundaries to the volume) at various sample synthesis temperatures T. The vertical lines mark the threshold values s_{th}. Large symbols correspond to the experimental data obtained in our works [6, 12, 13].

oxide films and zinc oxide films doped with 0.1 and 10 at % Mn [6]. The curves were obtained after the subtraction of the magnetic contribution from the substrate and sample holder. The magnetization is 2×10^{-3} μ_B/f.u. = 0.16 emu/g for zinc oxide films doped with 0.1 at % Mn, 0.8×10^{-3} μ_B/f.u. = 0.04 emu/g for zinc oxide films doped with 10 at % Mn, and 1×10^{-3} μ_B/f.u. = 0.06 emu/g for pure zinc oxide deposited on the aluminum substrate. Thus, owing to a very small grain size in our pore-free films (correspondingly, a high specific density of boundaries), the ferromagnetic behavior is observed in both doped and undoped zinc oxide films. The first signs of the ferromagnetic behavior of pure zinc oxide films were obtained only recently. Our paper [6] was the second reported work where ferromagnetism was observed in undoped zinc oxide.

The saturation magnetization increases linearly with the thickness (i.e., mass) of the zinc oxide film. The magnetization curves of zinc oxide films exhibit hysteresis with the coercive force H_c of about 0.02 T (zinc oxide film on a sapphire substrate, Fig. 7a) and about 0.01 T (zinc oxide film on an aluminum substrate, Fig. 7b). Figure 7 shows only the magnified central part of magnetization curves in order to clearly indicate the coercive force magnitude. The presented values are close to or exceed the coercive force ($H_c = 0.005$–0.02 T) observed in pure zinc oxide in works of other authors. At a temperature of 40 K, the saturation magnetization of pure zinc oxide films deposited on the sapphire substrate is only 40% larger than that at room temperature. This means that the Curie temperature of our films is much higher than room temperature.

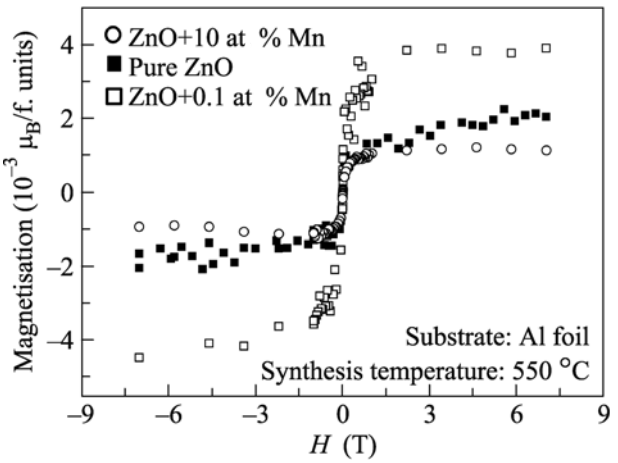

Fig. 6. Magnetization (in units of 10^{-3} μ_B/f.u.) of pure zinc oxide films and zinc oxide films doped with 0.1 and 10 at % Mn at room temperature [6].

EFFECT OF DOPING AND THE STRUCTURE OF GRAIN BOUNDARIES ON FERROMAGNETIC PROPERTIES OF ZINC OXIDE FILMS

All concentration dependences of the saturation magnetization J_s of zinc oxide doped with manganese [7], cobalt [12], or iron [13] are nonmonotonic (Fig. 8). The addition of first portions (0.02–0.12 at %) of a dopant is accompanied by an increase in the saturation magnetization by one–three orders of magnitude. We assume that an increase in the saturation magnetization at low dopant concentrations is associated with the injection of manganese, cobalt, or iron ions and corresponding charge carriers into pure zinc oxide. With a further increase in the dopant concentration, the saturation magnetization decreases rapidly and becomes almost indistinguishable from the background at 5 at % Mn, 22 at % Co, or 20 at % Fe. Then, the behaviors of the saturation magnetization are different. The saturation magnetization J_s for cobalt, which is characterized by only one oxidation degree, Co^{3+}, remains close to zero up to 42 at % Co (Fig. 8a). The saturation magnetization for iron, which can be present in the form of Fe^{2+} and Fe^{3+} ions in zinc oxide [23–26], increases again with the concentration (Fig. 8b). The saturation magnetization J_s for manganese, which is characterized by three oxidation degrees, +2, +3, and +4 [27–32], first increases and then decreases again (Fig. 8c). According to the known data, the dependence of the fraction of manganese or iron ions with various valences on the manganese or iron concentration, respectively, is complicated [23–32]. Thus, it seems reasonable that the concentration dependence of the saturation magnetization J_s becomes more complicated with an increase in the number of different oxidation degrees of doping ions (Fig. 8).

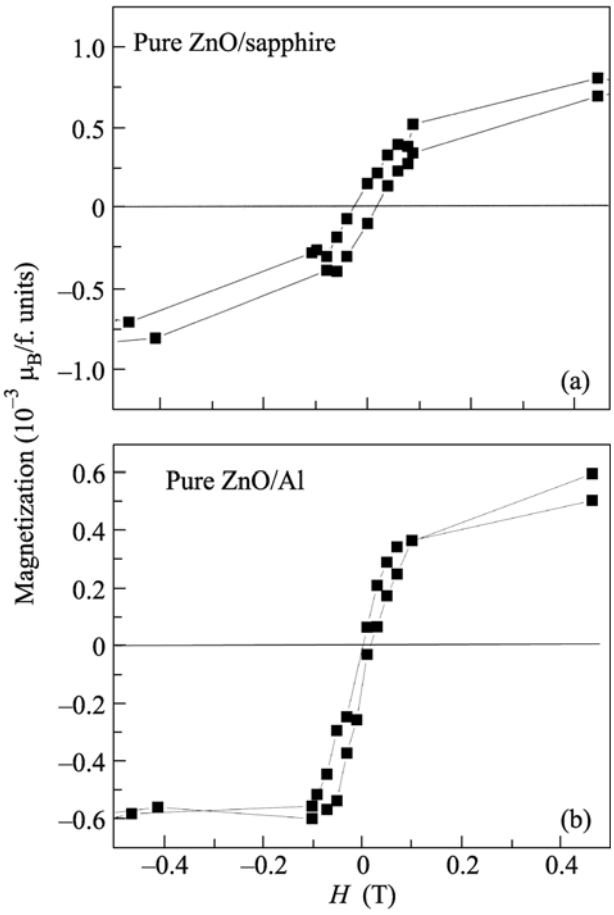

Fig. 7. Magnetic hysteresis at room temperature in pure zinc oxide films deposited on (a) a sapphire single crystal and (b) an aluminum foil [6]. Only the magnified central part of magnetization curves is shown in order to clearly indicate the coercive force magnitude.

A similar nonmonotonic behavior of the magnetization with an increase in the manganese, cobalt, or ion concentration was also observed in nanocrystalline manganese samples obtained by other methods (see references in [7, 12, 13]). However, the minima and maxima of the magnetization were located at other concentrations of dopants. This can be explained by different topologies of the grain boundary network in different materials.

Figure 9 shows bright-field micrographs obtained using high-resolution transmitting electron microscopy [8] for zinc oxide films doped with (a) 10 at % Mn and (b) 15 at % Mn. The direct resolution of the lattice makes it possible to observe grains of crystalline zinc oxide with a wurtzite lattice. Amorphous phase layers are clearly seen in Fig. 9a in the boundaries between these grains. Comparison of the structures in Figs. 9a and 9b indicates that the fraction of the amorphous phase increases with an increase in the manganese concentration from 10 to 15 at %. In particular, one of the zinc oxide grains with the wurtzite lattice in

Fig. 9a (in the center of the photograph) is completely surrounded by a Mn-enriched amorphous region. Amorphous layers in the sample with 15 at % Mn are already quite thick. This made it possible to obtain the pictures of Fourier transforms for amorphous and crystalline sections. The corresponding crystal grains (to the left and right) and amorphous layer (in the center) are marked by letters *A*, *B*, and *C* in Fig. 9b.

Figure 9 clearly demonstrates what occurs upon the gradual addition of manganese to nanocrystalline zinc oxide. Some doping manganese atoms get into the crystal lattice of grains and make a contribution to the shift of X-ray diffraction peaks from the coherent scattering regions (grains with the wurtzite lattice). Other manganese atoms (approximately 2/3 of the total number of atoms) get into amorphous layers surrounding grains and separating them. The thickness of these amorphous layers increases with the manganese concentration. Our quantitative estimate in [5] showed that, at 30 at % Mn (when the solubility limit for a grain size of 20 nm is reached), the thickness of grain boundary layers is 6–10 ML of manganese oxide and the thickness of layers on the outer surface is 2 ML. Such a situation can significantly differ from the case of the McLean single-layer adsorption (on the surface or in the grain boundaries).

The morphology of Mn-enriched amorphous regions between zinc oxide grains strongly differs from very homogeneous and uniformly thin amorphous layers of grain boundary prewetting phases in $ZnO:Bi_2O_3$ samples obtained by the liquid-phase sintering method [33]. In particular, amorphous regions in the sample with 15 at % Mn (Fig. 9b) completely surround some zinc oxide grains and only partially enter between other grains. Such a microstructure is very similar to the morphology of two-phase polycrystals, where the second phase completely wets some boundaries and partially wets other boundaries.

According to the experiments with metal alloys, it is well known that the distribution of grain boundaries over misorientations and inclinations significantly changes the properties of polycrystals. We compare the magnetic properties of zinc oxide nanocrystalline films with the same grain size (which was much smaller than the threshold value), but with a different distribution of boundaries over misorientations and inclinations (or so-called grain boundary character distribution).

Figure 10 shows the X-ray diffraction spectra for zinc oxide thin films that are deposited on the sapphire single crystals with the (102) orientation and are annealed in (upper line) air and (lower line) argon [9]. The X-ray spectrum for the film annealed in argon contains three peaks corresponding to the 100, 002, and 101 reflections of the hexagonal wurtzite lattice of zinc oxide. The X-ray spectrum for the film annealed in air contains only one peak corresponding to the 002 reflection from zinc oxide with the hexagonal wurtzite structure. This means that the film synthesized in air has a strong texture.

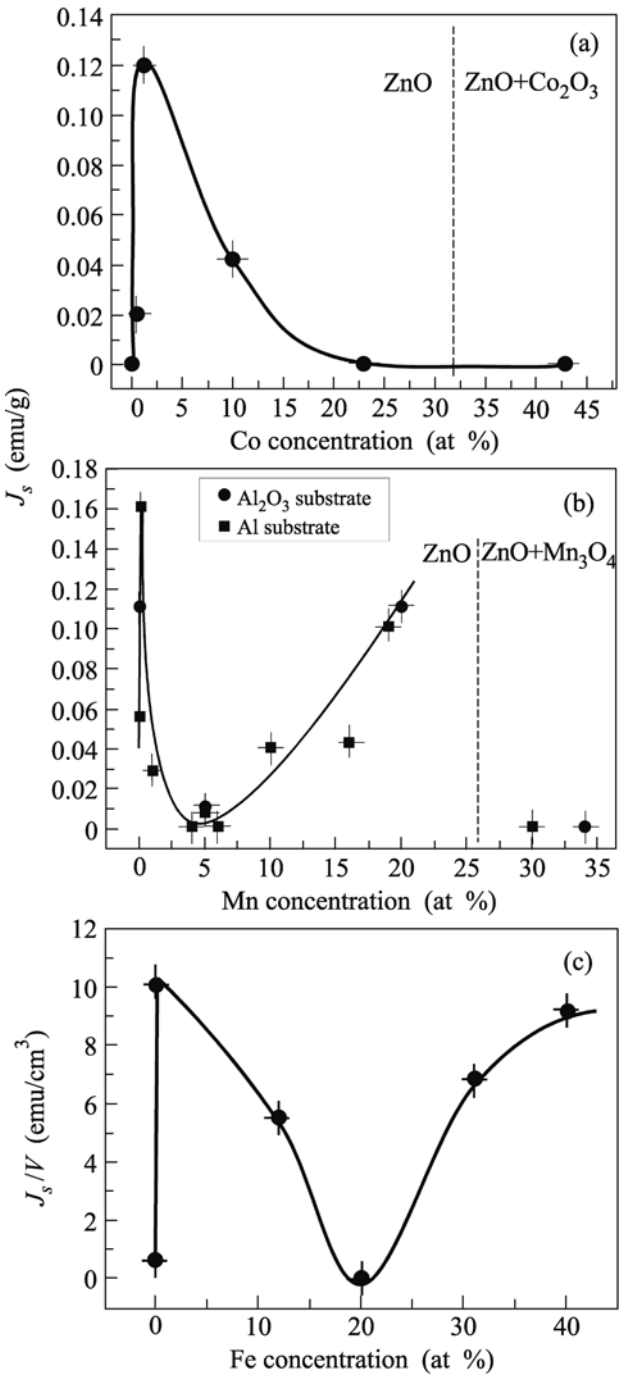

Fig. 8. Saturation magnetization of doped zinc oxide films versus the (a) cobalt [12], (b) manganese [7], and (c) iron [13] concentration.

Figure 11 shows the magnetization curves for zinc oxide thin films annealed in (closed triangles) air and (closed circles) argon [9]. Open circles show the magnetization curve for the bare sapphire substrate. The

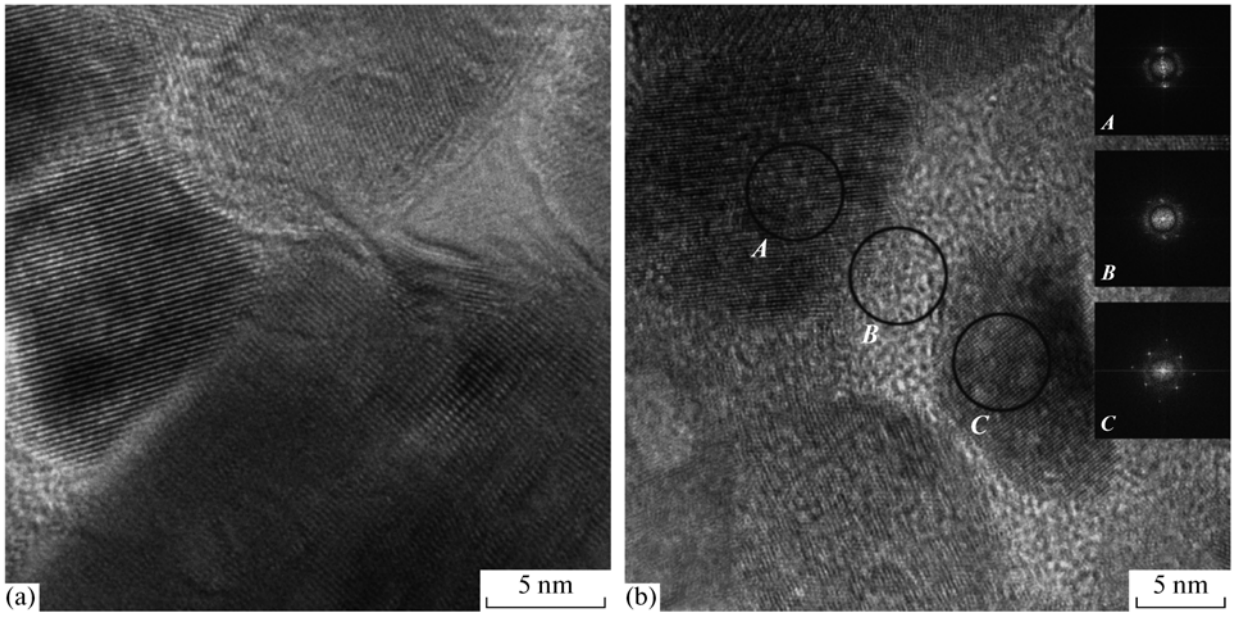

Fig. 9. Brightfield micrographs obtained using high-resolution transmitting electron microscopy [8] for zinc oxide films doped with (a) 10 at % Mn, amorphous layers between crystalline ZnO nanograins, and (b) 15 at % Mn, crystalline ZnO nanograins surrounded by amorphous layers. The insets show the Fourier transforms for amorphous and crystalline sections.

film annealed in air has pronounced ferromagnetic properties with a saturation magnetization of 12×10^{-6} emu (at applied fields above 6 T). The film annealed in argon has no ferromagnetic properties and remains diamagnetic. (Ferromagnetism of the substrate is determined by residual ferromagnetic impurities.) Comparison of these two curves (closed and open circles) shows that the zinc oxide film annealed in argon hardly has any additional ferromagnetism as compared to the substrate.

Comparison of Figs. 10 and 11 shows that the zinc oxide film with a strong texture has ferromagnetic properties, whereas the untextured (or weakly textured) film remains diamagnetic. These results demonstrate that the ferromagnetic behavior of zinc oxide is determined not only by the specific area of grain

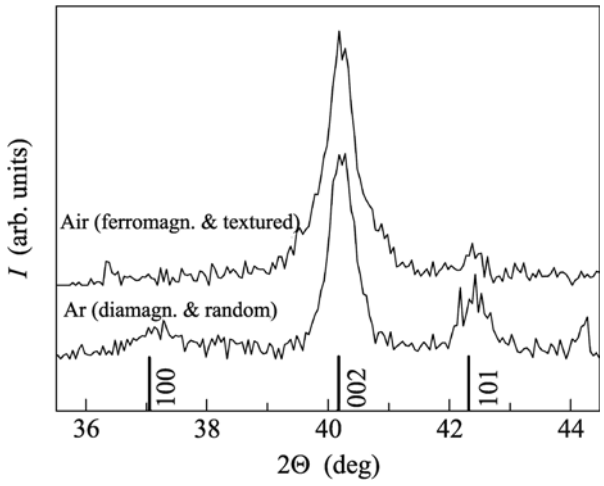

Fig. 10. X-ray diffraction curves for the (upper line) ferromagnetic and (lower line) diamagnetic zinc oxide thin films that are deposited on the sapphire substrate with the (102) orientation and are annealed in (upper line) air and (lower line) argon [9].

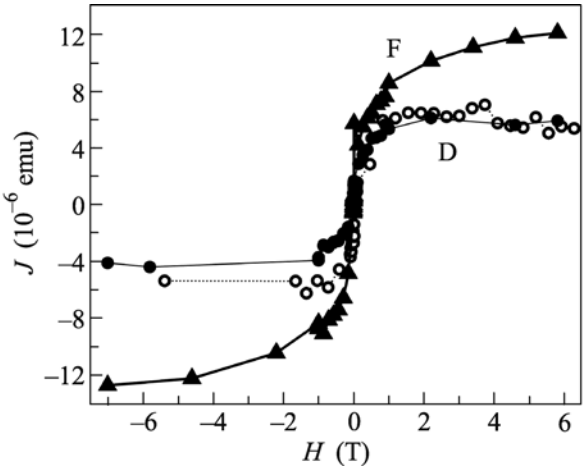

Fig. 11. Magnetization curves for thin zinc oxide films annealed in air (F, ferromagnetic films, closed triangles) and in argon (D, diamagnetic films, closed circles) [9]. Open circles show the magnetization curve for the bare sapphire substrate.

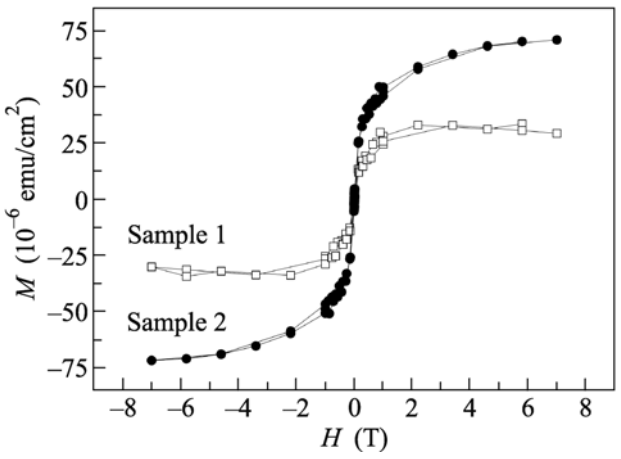

Fig. 12. Magnetization curves $M(H)$ at room temperature for thin zinc oxide films in samples (open squares) 1 and (closed circles) 2. The magnetization was measured together with the sapphire substrate [10].

boundaries per unit volume of nanocrystalline films. Even if the grain size is much smaller than the critical value necessary for the observation of ferromagnetism in pure zinc oxide, the ferromagnetic behavior depends on whether the film is textured. Thus, the ferromagnetism of zinc oxide depends not only on the presence of grain boundaries but also on their structure.

Furthermore, we studied undoped zinc oxide films obtained by thermal pyrolysis from butanoate precursors in an argon atmosphere at 650°C for 0.5 h (sample 1) and at 550°C for 24 h (sample 2) [10]. The thicknesses of these films were 690 and 370 nm, respectively. Figure 12 shows the magnetization curves $M(H)$ for these films. The magnetization was measured with the sapphire substrate. The magnetization values are reduced to the same area and are given in electromagnetic units per centimeter squared. It is clearly seen that the ferromagnetic properties of sample 2 are more pronounced.

Figure 13 shows the bright-field high-resolution electron microscope image for the zinc oxide film annealed in argon at 650°C for 0.5 h (sample 1) [11]. This sample exhibits very weak ferromagnetism with $M_s(1) = 27 \times 10^{-6}$ emu/cm^2 (Fig. 12a). Zinc oxide crystal grains are separated from each other by a thin (2–5 nm) amorphous film. The electron diffraction pattern includes the reflection for the wurtzite phase of zinc oxide and a weak halo of the amorphous phase (Fig. 13b). Figure 14a shows the microstructure of the zinc oxide film annealed in argon at 550°C for 24 h (sample 2). This film has the ferromagnetic properties with the saturation magnetization $M_s(2) = 75 \times 10^{-6}$ emu/cm^2 (Fig. 12a). It is clearly seen in the micrograph that zinc oxide crystal grains with the wurtzite structure are surrounded by wide amorphous layers. The electron diffraction pattern (Fig. 14b) includes reflections for the wurtzite lattice and a strong halo of the amorphous phase.

Thus, the saturation magnetization of ferromagnetic zinc oxide samples increases distinctly with the

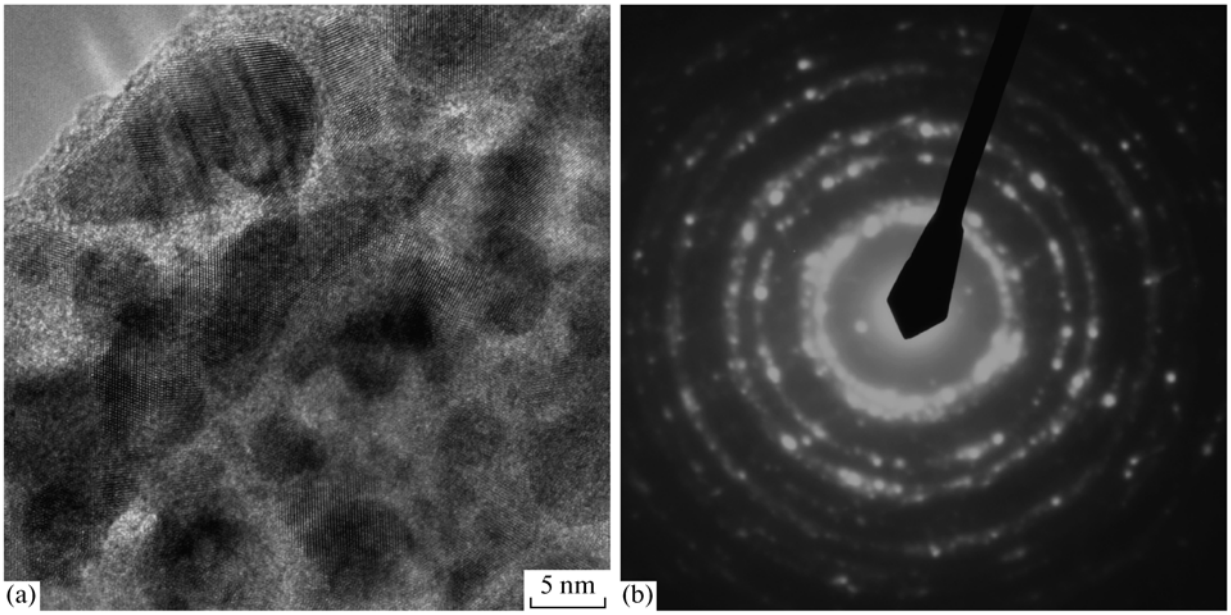

Fig. 13. (a) Bright-field high-resolution electron microscope image for the zinc oxide film annealed in argon at 650°C for 0.5 h (sample 1). Zinc oxide crystal grains separated from each other by a thin (2–5 nm) amorphous film can be seen. (b) Electron diffraction pattern. Reflections for the wurtzite phase of zinc oxide and a weak halo of the amorphous phase can be seen [11].

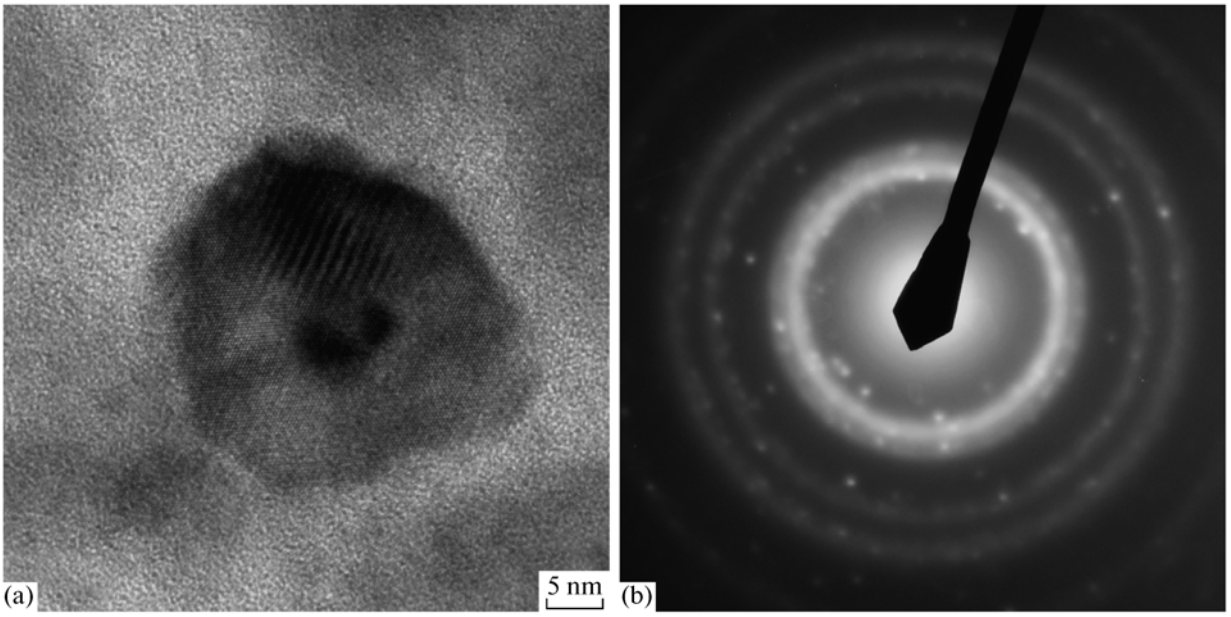

Fig. 14. (a) Bright-field high-resolution electron microscope image for the zinc oxide film annealed in argon at 550°C for 24 h (sample 2). Zinc oxide crystal grains are surrounded by wide amorphous layers. (b) Electron diffraction pattern. Reflections for the wurtzite lattice and a strong halo of the amorphous phase can be seen [11].

fraction of the amorphous phase between zinc oxide crystal grains. The concentration dependences of the saturation magnetization in doped zinc oxide nanocrystalline samples fabricated by various methods are different for manganese [7], cobalt [12], and iron [13]. Nonuniformly distributed defects of the crystal lattice are apparently insufficient for the appearance of ferromagnetism in zinc oxide. Moreover, the correct combination and topology of the mutually penetrating crystalline and amorphous phases are necessary for the appearance of the ferromagnetic properties in pure zinc oxide.

To conclude, it is noteworthy that grain boundaries not only lead to the shift of the solubility limit with a decrease in the grain size in zinc oxide but also are responsible for its ferromagnetic behavior. Not only a high specific density of grain boundaries (their quantity) but also the structure of grain boundaries, as well as the distribution of boundaries over the orientations and disorientations (their quality), is important.

This work was supported by the Russian Foundation for Basic Research (project no. 10-02-00086).

REFERENCES

1. T. Dietl, H. Ohno, F. Matsukura, et al., Science **287**, 1019 (2000).
2. T. Dietl, Nature Mater. **9**, 965 (2010).
3. B. Straumal, A. Mazilkin, P. Straumal, et al., Int. J. Nanomanufact. **2**, 253 (2008).
4. B. B. Straumal, A. A. Mazilkin, S. G. Protasova, et al., Acta Mater. **56**, 6246 (2008).
5. B. B. Straumal, B. Baretzky, A. A. Mazilkin, et al., J. Eur. Ceram. Soc. **29**, 1963 (2009).
6. B. B. Straumal, A. A. Mazilkin, S. G. Protasova, et al., Phys. Rev. B **79**, 205206 (2009).
7. B. B. Straumal, S. G. Protasova, A. A. Mazilkin, et al., J. Appl. Phys. **108**, 073923 (2010).
8. B. B. Straumal, A. A. Myatiev, P. B. Straumal, et al., JETP Lett. **92**, 396 (2010).
9. B. B. Straumal, A. A. Mazilkin, S. G. Protasova, et al., Phys. Status Solidi B **248**, 581 (2011).
10. B. B. Straumal, A. A. Mazilkin, S. G. Protasova, et al., Thin Solid Films **520**, 1192 (2011).
11. B. B. Straumal, S. G. Protasova, A. A. Mazilkin, et al., Mater. Lett. **71**, 21 (2012).
12. B. B. Straumal, A. A. Mazilkin, S. G. Protasova, et al., Phil. Mag. **93**, 1371 (2013).
13. B. B. Straumal, S. G. Protasova, A. A. Mazilkin, et al., Beilstein J. Nanotechnol. **4** (2013, in press).
14. D. McLean, *Grain Boundaries in Metals* (Clarendon, Oxford, 1957).
15. M. L. Trudeau, J. Y. Huot, and R. Schulz, Appl. Phys. Lett. **58**, 2764 (1991).
16. K. Suzuki, A. Makino, A. Inoue, et al., J. Appl. Phys. **70**, 6232 (1991).
17. V. Heera, K. N. Madhusoodanan, W. Skorupa, et al., J. Appl. Phys. **99**, 123716 (2006).
18. B. B. Straumal, S. V. Dobatkin, A. O. Rodin, et al., Adv. Eng. Mater. **13**, 463 (2011).
19. C. Lemier, and J. Weissmuller, Acta Mater. **55**, 1241 (2007).
20. A. Rizea, D. Chirlesan, C. Petot, et al., Solid State Ionics **146**, 341 (2002).

21. D. F. Wang, S. Y. Park, H. W. Lee, et al., Phys. Status Solidi A **204**, 4029 (2007).
22. N. Gopalakrishnan, J. Elanchezhiyan, K. P. Bhuvana, et al., Scr. Mater. **58**, 930 (2008).
23. H. Liu, J. Yang, Y. Zhang, et al., Phys.: Condens. Matter **21**, 145803 (2009).
24. P. Wu, G. Saraf, Y. Lu, et al., Appl. Phys. Lett. **89**, 012508 (2006).
25. Y. Lin, D. Jiang, F. Lin, et al., J. Alloys Comp. **436**, 30 (2007).
26. D. Karmakar, S. K. Mandal, R. M. Kadam, et al., Phys. Rev. B **75**, 144404 (2007).
27. C. J. Cong and K. L. Zhang, Phys. Status Solidi A **243**, 2764 (2006).
28. P. Thakur, K. H. Chae, J.-Y. Kim, et al., Appl. Phys. Lett. **91**, 162503 (2007).
29. P. Abbamonte, L. Venama, A. Rusydi, et al., Science **297**, 581 (2002).
30. E. Pellegrin, N. Nucker, J. Fink, et al., Phys. Rev. B **47**, 3354 (1993).
31. K. Asokan, J. C. Jan, K. V. R. Rao, et al., J. Phys.: Condens. Matter **16**, 3791 (2004).
32. J.-H. Guo, A. Gupta, P. Sharma, et al., J. Phys.: Condens. Matter **19**, 172202 (2007).
33. H. Wang and Y.-M. Chiang, J. Am. Ceram. Soc. **81**, 89 (1998).

Translated by R. Tyapaev